

Effects of segregated Cu on an Fe grain boundary by first-principles tensile tests

Motohiro Yuasa* and Mamoru Mabuchi

Department of Energy Science and Technology, Graduate School of Energy Science, Kyoto University,

Yoshidahonmachi, Sakyo-ku, Kyoto 606-8501, Japan

*Corresponding Author (Email address: yuasamotohiro@t03.mbox.media.kyoto-u.ac.jp).

Abstract

Cu is known as one of the harmful tramp elements in recycled Fe. In the present work, the effects of

Cu on Fe grain boundary (GB) embrittlement have been investigated by first-principles tensile tests.

Because the Fe-Cu bonds are rather isotropic and the effects due to their difference in atomic size are

negligibly small, the GB atomic structure prior to straining is little changed by Cu segregation.

However, the Fe-Fe bond around the Cu atom is weakened due to charge transfer from the Fe atom to

the Cu atom, and premature bond-breaking occurs at the weakened Fe-Fe bond, resulting in an

enhancement of GB embrittlement by Cu segregation. The *s* and *p* electrons play a vital role in the

charge transfer.

PACS: 62.20.-x, 68.35.Dv, 81.05.Bx

Submitted to Journal of Physics: Condensed Matter

1. Introduction

When Fe scrap is recycled as a material resource, tramp elements such as Cu and Sn tend to remain in the recycled Fe since these elements are difficult to eliminate. In particular, the amount of Cu remaining in recycled Fe is increasing rapidly because a large amount of Cu is used as electric leads in vehicles. The remaining Cu often causes hot shortness [1-4]. Seo *et al.* [1] suggested that hot shortness is related to grain boundary (GB) embrittlement due to the penetration of Cu-enriched liquid phases into the Fe GB. The harmful effects of liquid phases on the GB cohesion depend on the wetting of the GB [5-7]. Pharr *et al.* [5] showed that the effects of intergranular liquid phases on the compression creep behavior are negligibly small when the wetted GB area is less than 70%. Therefore, a large amount of intergranular Cu impurities is required for GB embrittlement induced by liquid phases.

On the other hand, it is well known that small amounts of intergranular impurities such as S, P and so on enhance the embrittlement of Fe GBs. First-principles studies have demonstrated that the enhanced GB embrittlement is due to the charge transfer [8-14] and the reduced bond mobility [15-19]. Thus, another possibility for the hot shortness is GB embrittlement enhanced by intergranular Cu segregation. Seah [20] suggested that Cu segregation as well as P segregation can induce the GB embrittlement of Fe. However, to the authors' knowledge, there are no first-principles studies on the GB embrittlement by intergranular Cu segregation. Recently, the first-principles tensile tests have been performed to investigate the variation in the atomic and electronic structures of GBs with

impurity segregation with strain [10,11,21,22]. The embrittlement behavior depends on the spatial anisotropy of the bonding between the impurity atom and the surrounding host atoms [18,19]. Hence, it is worthwhile to investigate the variation of bonding characteristics with strain. In the present work, first-principles tensile tests are performed on Fe with a Cu-segregated GB and with a non-segregated GB.

2. Computational method

Two bcc Fe cells with a $\Sigma 3$ (111)/[1 $\bar{1}$ 0] tilt GB were used for the first-principles tensile tests: one was a cell without Cu segregation at the GB (clean GB model) and the other was a cell with Cu segregation at the GB (Cu-segregated GB model), in which an Fe atom (Fe2) at the GB was substituted with a Cu atom, as shown in figure 1. The initial cell size was 4.05 x 7.02 x 14.89 Å. Geometry optimization calculations were performed using the Cambridge Serial Total Energy Package (CASTEP) [23], in which density functional theory (DFT) [24,25] was used with a plane wave basis set to calculate the electronic properties of solids from the first principles. The exchange–correlation interactions were treated using the spin-polarized version of the generalized gradient approximation within the scheme due to Perdew-Burke-Ernzerhof [26]. Ultrasoft pseudopotentials [27] represented in reciprocal space were used for all elements in the calculations. The cutoff energy was set at 300 eV. The Brillouin zone was sampled using a Monkhorst-Pack 6 x 4 x 2 k-point mesh and Gaussian smearing with 0.1 eV width. The simulation conditions such as the cutoff energy, sampling k-points

and Gaussian smearing in our study are determined on the base of Ref. [13]

After the geometry optimization calculation including the cell optimization, a uniaxial tensile strain with an increment of 2% in the [111] direction, which was normal to the GB plane, was applied to the cells in the first-principles tensile tests. The lattice dimensions in the GB plane were fixed, neglecting the Poisson's ratio to simplify the calculation [11,22]. This step was repeated until the GB fracture occurred. In each step, all atomic positions were optimized in accordance with Hellman-Feynman forces until all the forces were less than 0.03 eV/Å. In the present work, the bond-breaking was determined from a rapid increase in the bond length.

3. Results and discussion

3.1. Tensile strength and fracture behavior

Figure 2 (a) shows the [111] stress-strain curves for the clean GB and Cu-segregated GB models, where the [111] stress is the tensile stress in the [111] direction which is parallel to the tensile direction. In the clean GB model, the tensile stress increases to about 25 GPa with increasing strain until the strain reaches 24%. The flow stress is nearly constant in the strain range of 24-28%, then the stress decreases rapidly at 28-30%, and finally, GB fracture occurs at 30%. In the Cu-segregated GB model, the tensile stress increases to about 23 GPa until the strain reaches 20%, then the stress decreases rapidly at 20-22% and GB fracture occurs at 22%. Thus, the tensile strength and the strain to failure in the Cu-segregated GB model are 8% and 27% lower than those in the clean GB model, respectively.

Note that both the tensile strength and the strain to failure are reduced by Cu segregation in the Fe GB.

To verify that Cu is an embrittler in the Fe GB, the difference between the segregation energies at the GB ($=\Delta E_{GB}$) and at the free surface ($=\Delta E_{SF}$) was calculated according to the Rice-Wang thermodynamics model [28]. As a result, $\Delta E_{GB} - \Delta E_{SF}$ was 0.66 eV/atom for Cu segregation in Fe. This is in accord with the results in figure 2 (a). Figure 2 (b) shows the $[11\bar{2}]$ stress-strain curves, where the $[11\bar{2}]$ stress is the stress in the $[11\bar{2}]$ direction which is parallel to the GB and the strain is the strain in the $[111]$ direction. In the clean GB model, after the $[11\bar{2}]$ stress increases until the strain reaches 28%, it decreases rapidly at 28-30%. On the other hand, in the Cu-segregated GB model, the $[11\bar{2}]$ stress increases until the strain reaches 20%, then it decreases rapidly at 20-22%. The same trend was found in the $[1\bar{1}0]$ stress as well as the $[11\bar{2}]$ stress. These behaviors of the stresses parallel to the GB corresponds to those of the $[111]$ stress parallel to the tensile direction.

Kohyama and coworkers [11] showed by first-principles tensile tests on an Al GB segregated by Na or Ca that a large residual compressive stress is generated prior to straining due to the larger atomic radii of Na and Ca than that of Al, resulting in a reduction in tensile strength. In the present work, there is little difference in atomic radius between Fe ($=0.124$ nm) and Cu ($=0.128$ nm). Hence, the enhancement of GB embrittlement by Cu segregation originates from only the chemical contribution. On the other hand, S-induced embrittlement is related to the weak bonds between the S atom and the neighboring host atoms due to the anisotropic bonding [29]. In this case, the flow stress for the segregated GB is lower than that for the clean GB from the initial stage of straining, in spite of the

absence of residual compressive stress [30]. As shown in figure 2, however, the flow stress in the Cu-segregated GB model is almost the same as that in the clean GB model up to the strain of 20%, suggesting that the Fe-Cu bonds are isotropic. The trend of no effects of impurity segregation on the flow stress has been also found in segregated Ga on an Al GB [31], where the embrittlement is enhanced by the charge transfer from the host atom to the impurity atom [32].

3.2. Bond length

The variations in the bond lengths of the (a) Fe1-Fe3, (b) Fe1-Fe2(Cu), (c) Fe4-Fe2(Cu) and (d) Fe5-Fe2(Cu) as a function of strain are shown in figure 3. Prior to straining, the bond lengths of Fe1-Fe3, Fe1-Cu and Fe4-Cu in the Cu-segregated GB model are almost the same as those of Fe1-Fe3, Fe1-Fe2 and Fe4-Fe2 in the clean GB model, although the bond length of Fe5-Cu in the Cu segregated GB model is a little shorter than that of Fe5-Fe2 in the clean GB model. This verifies that the Fe-Cu bonds are considerably isotropic. The differences in bond length between Fe1-Fe2 and Fe1-Cu, between Fe4-Fe2 and Fe4-Cu, and between Fe5-Fe2 and Fe5-Cu remain minor until just before bond breaking; however, Fe1-Fe3 in the Cu-segregated GB model exhibits a greater increase in length than Fe1-Fe3 in the clean GB model. In the Cu-segregated GB model, the Fe1-Cu, Fe4-Cu and Fe5-Cu are broken soon after the Fe1-Fe3 bond breaking occurs. This is because the Fe-Cu bonds are isotropic. However, in the case of the P-segregated GB where Fe-P bond is anisotropic [33], the first bond breaking occurs at the Fe-P bond, and thereafter, the second bond breaking occurs at Fe-Fe bond.

Either Fe3-Cu bond breaking or Fe1-Cu bond breaking is enough for GB fracture. In the present work, the Fe1-Cu bond breaking occurs, therefore, the Cu-Fe3 bond breaking does not occur. Also, the threshold bond length for bond breaking, which is the bond length just before a rapid increase of bond length, is 3.18 Å for the Fe1-Fe3 in the clean GB model and 2.96 Å for the Fe1-Fe3 in the Cu-segregated GB model, respectively. Thus, the threshold bond length for bond breaking of Fe1-Fe3 in the Cu-segregated GB model is shorter than that in the clean GB model. Note that the Cu atom weakens the Fe-Fe bond around the Cu atom, while it has minor effects on all the Fe-Cu bonds. The bond breaking occurs at the strain of 20% not only at the Fe1-Fe3 bond but also at the Fe-Cu bonds, corresponding to the stress-strain curve in figure 2.

3.3. Charge density distribution and density of states

Figure 4 shows the charge density distribution of $(\bar{1}\bar{1}0)$ at the strains of 0%, 10% and 20%. The Fe1-Fe3 bond length prior to straining in the Cu-segregated GB model was almost the same as that in the clean GB model, as shown in figure 3. However, it appears from figure 4 that the charge density of the Fe1-Fe3 bond prior to straining in the Cu-segregated GB model is a little lower than that in the clean GB model. Figure 5 shows the charge density difference of $(\bar{1}\bar{1}0)$ between the Cu-segregated GB model and the non-segregated GB model. In the non-segregated GB model, the Cu atom is replaced by a Fe atom with the same atomic configuration. It can be seen from figure 5 that a reduced charge density of Fe1-Fe3 bond in the Cu-segregated GB model originates from the chemical

contribution. As shown in figure 4, the difference in the charge density of the Fe1-Fe3 bond between the Cu-segregated GB model and the clean GB model increases increasing the strain. The premature bond-breaking of Fe1-Fe3 in the Cu-segregated GB model can clearly be attributed to a reduction in its charge density. The Fe5-Cu length prior to straining in the Cu-segregated GB model was slightly shorter than the Fe5-Fe2 length in the clean GB model, as shown in figure 3. However, the charge density around the Fe5 in the Cu-segregated GB model tends to be lower than that in the clean GB model (figure 6). This leads to the larger rate of increase of the Fe5-Cu length with increasing strain than that of the Fe5-Fe2 length, resulting in the premature bond-breaking of Fe5-Cu.

Figure 7 shows the partial density of states (PDOS) for the Fe1 atom. The PDOS in the Cu-segregated GB model is almost the same as that in the clean GB model, and no hybridization peaks are found in the Cu-segregated GB model. It is therefore suggested that the Fe-Cu bond is a metallic bond without covalent characteristics. The occupation numbers in the $3d$, $4s$ and $4p$ electrons of the Fe1 atom are listed in Table 1. It can be seen that charge transfer from the Fe atom to the Cu atom occurs. Clearly, the weakened Fe-Fe bond around the Cu atom is due to the charge transfer. It is of interest to note that the numbers of $4s$ and $4p$ electrons in the Fe atom are decreased by the Cu atom, while the number of $3d$ electrons hardly changes [34]. This trend of charge transfer remained unchanged until just before the bond breaking.

The calculated magnetic moment of each atom at the strain of 0% is listed in Table 2. It can be seen that the Cu atom enhances the magnetic moment of neighboring Fe atoms [35]. Figure 8 shows

the up- and down-spin PDOS of *d*-bands for the Fe1 atom. The *d*-band in the Cu-segregated GB model is narrow, compared with that in the clean GB model, resulting in an enhancement of the magnetic moment [36]. Also, inspection of figure 8 reveals that the number of electrons of occupied states for down-spin is reduced in the Cu-segregated GB model, compared with that in the clean GB model. Freeman and colleagues [37] showed that the magnetic moment of Fe atoms is decreased by an increase in number of electrons in the down-spin states. Therefore, the enhanced magnetic moment of Fe atoms in the Cu-segregated GB model is due to the narrowed *3d* band and the reduced electrons in the down-spin state.

The H atom is a strong embrittler in the Fe GB [38], where the segregated H atom induces charge transfer from the Fe atoms to itself [39,40]. H is a strong acceptor of electrons because the electronegativity of H (= 2.20 [41]) is much larger than that of Fe (= 1.83 [41]). Note that Cu is also an electron acceptor, although the difference (= 0.07) in electronegativity between Cu and Fe is much lower than that between H and Fe (= 0.37). Freeman and coworkers [18,19] showed that P in Fe is not an acceptor, in spite of their large difference in electronegativity (= 0.36). It can be seen from Table 1 that the electrons with isotropic orbitals play a vital role in the charge transfer from the Fe atom to the Cu atom, indicating that the charge accumulation depends on the anisotropy of bonding, namely, for anisotropic bonding, the charge accumulation tends to occur as a result of covalent-like or electrovalent-like bonding [42]; on the other hand, for isotropic bonding, the charge transfer can be induced by a difference in electronegativity. It is therefore likely that because Fe-Cu bonds are

isotropic, the charge transfer is driven by a difference in electronegativity, unlike Fe-P bonds.

4. Conclusions

The effects of Cu on Fe GB embrittlement have been studied by the first-principles tensile tests. Because the Fe-Cu bonds are rather isotropic and the difference in atomic size between Fe and Cu is minor, the GB atomic structure prior to straining is little changed by Cu segregation. However, the Fe-Fe bond around the Cu atom is weakened due to charge transfer from the Fe atom to the Cu atom and premature bond-breaking occurs at the weakened Fe-Fe bond, resulting in an enhancement of GB embrittlement by Cu segregation. The charge transfer is induced, in spite of a small difference in electronegativity between Fe and Cu, because the *s* and *p* electrons play a vital role in the charge transfer.

Acknowledgements

This work was supported from Japan Society for the Promotion of Science (Grant No. 22·5568). Computation time was provided by the SuperComputer Laboratory, Institute for Chemical Research, Kyoto University.

References

- [1] Seo S J, Asakura K and Shibata K 1997 *ISIJ Int.* **37** 232
- [2] Imai N, Komotsubara N and Kunishige K 1997 *ISIJ Int.* **37** 217
- [3] Matsuoka H, Osawa K, Ono M and Ohmura M 1997 *ISIJ Int.* **37** 255
- [4] Hasegawa H, Nakajima K and Mizoguchi S 2003 *ISIJ Int.* **43** 1021
- [5] Pharr G M, Godavarti P S and Vaandrager B L 1989 *J. Mater. Sci.* **24** 784
- [6] Vaandrager B L and Pharr G M 1989 *Acta Metall.* **37** 1057
- [7] Bordeaux F, Dang M C and Baudelet B 1994 *J. Mater. Sci.* **29** 3023
- [8] Briant C L and Messmer R P 1980 *Phil. Mag. B* **42** 569
- [9] Messmer R P and Briant C L 1982 *Acta Metall.* **30** 457
- [10] Geng W T, Freeman A J and Olson G B 2001 *Phys. Rev. B* **63** 165415
- [11] Lu G H, Zhang Y, Deng S, Wang T, Kohyama M, Yamamoto R, Liu F, Horikawa K and Kanno M 2006 *Phys. Rev. B* **73** 224115
- [12] Yamaguchi M, Shiga M and Kaburaki H 2005 *Science* **307** 393
- [13] Yamaguchi M, Nishiyama Y, Kaburaki H 2007 *Phys. Rev. B* **76** 035418
- [14] Yang R, Zhao D L, Wang Y M, Wang S Q, Ye H Q and Wang C Y 2001 *Acta Mater.* **49** 1079
- [15] Haydock R 1981 *J. Phys. C: Solid State Phys.* **14** 3807
- [16] Goodwin L, Needs R J and Heine V 1988 *Phys. Rev. Lett.* **60** 2050
- [17] Goodwin L, Needs R J and Heine V 1990 *J. Phys.: Condens. Matter* **2** 351

- [18] Wu R, Freeman A J and Olson G B 1994 *Science* **265** 376
- [19] Wu R, Freeman A J and Olson G B 1994 *Phys. Rev. B* **50** 75
- [20] Seah M P 1980 *Acta Metall.* **28** 955
- [21] Ogata S, Umeno Y and Kohyama M 2009 *Modell. Simul. Mater. Sci. Eng.* **17** 013001
- [22] Lu G H, Deng S, Wang T, Kohyama M and Yamamoto R 2004 *Phys. Rev. B* **69** 134106
- [23] Payne M C, Teter M P, Allan D C, Arias T A and Joannopoulos J D 1992 *Rev. Mod. Phys.* **64** 1045.
- [24] Hohenberg P and Kohn W 1964 *Phys. Rev.* **136** B864
- [25] Kohn W and Sham L 1965 *Phys. Rev.* **140** A1133
- [26] Perdew J P, Burke K and Ernzerhof M 1996 *Phys. Rev. Lett.* **77** 3865
- [27] Vanderbilt D 1990 *Phys. Rev. B* **41** 7892
- [28] Rice J R and Wang J S 1989 *Mater. Sci. Eng. A* **107** 23
- [29] Lu G H, Kohyama M and Yamamoto R 2003 *Philos. Mag. Lett.* **83** 159
- [30] Zhang Y, Lu G H, Deng S, Wang T, Xu H, Kohyama M and Yamamoto R 2007 *Phys. Rev. B* **75** 174101
- [31] Zhang Y, Lu G H, Wang T, Deng S, Kohyama M and Yamamoto R 2006 *Mater. Trans.* **47** 2678
- [32] Zhang Y, Lu G H, Wang T, Deng S, Shu X, Kohyama M and Yamamoto R 2006 *J. Phys.: Condens. Matter* **18** 5121
- [33] Yuasa M and Mabuchi M 2010 *Phys. Rev. B* **82** 094108
- [34] Shang J X, Zhao X D, Wang F H, Wang C Y and Xu H B 2006 *Comput. Mater. Sci.* **38** 217

- [35] Rahman G, Kim I G, Bhadeshia H K D H and Freeman A J 2010 *Phys. Rev. B* **81** 184423
- [36] Tischer M, Hjortstam O, Arvanitis D, Dunn J H, May F, Baberschke K, Trygg J, Wills J M, Johansson B and Eriksson O 1995 *Phys. Rev. Lett.* **75** 1602
- [37] Wu R, Freeman A J and Olson G B 1992 *J. Mater. Res.* **7** 2403
- [38] Hirth J P 1980 *Metall. Trans. A* **11** 861
- [39] Zhong L, Wu R and Freeman A J 2000 *Phys. Rev. B* **62** 13938
- [40] Itsumi Y and Ellis D E 1996 *J. Mater. Res.* **11** 2214
- [41] Allred A L 1961 *J. Inorg. Nucl. Chem.* **17** 215
- [42] Uesugi T, Kohyama M and Higashi K 2003 *Phys. Rev. B* **68** 18410

Captions

Table 1 Occupation numbers in $3d$, $4s$ and $4p$ electrons of the Fe1 atom in the clean GB model and the Cu-segregated GB model. Note that the $4s$ and $4p$ electrons play a vital role in the charge transfer.

Table 2 Calculated magnetic moment (in units of μ_B) of each atom in the clean GB and Cu-segregated GB models.

Figure 1 Unit cell model of Fe with a $\Sigma 3$ $(111)/[1\bar{1}0]$ tilt grain boundary. In the present work, two cells are used: one is a cell without Cu segregation at the grain boundary (clean GB model) and the other is a cell with Cu segregation at the grain boundary (Cu-segregated GB model) in which an Fe atom (Fe2) at the grain boundary is substituted with a Cu atom. The initial cell size is $4.05 \times 7.02 \times 14.89$ Å. The blue and dark blue circles indicate the Fe atoms on the $(1\bar{1}0)$ and the $(2\bar{2}0)$ planes, respectively.

Figure 2 Stress-strain curves for the clean GB and Cu-segregated GB models, (a) $[111]$ stress-strain curves and (b) $[11\bar{2}]$ stress-strain curves, where the $[111]$ stress is the tensile stress in the $[111]$ direction which is parallel to the tensile direction, the $[11\bar{2}]$ stress is the stress in the

[11 $\bar{2}$] direction which is parallel to the GB and the strain is the strain in the [111] direction.

Note that the tensile strength and the strain to failure in the Cu-segregated GB model are 8% and 27% lower than those in the clean GB model, respectively.

Figure 3 Variations in bond length as a function of strain, (a) Fe1-Fe3, (b) Fe1-Fe2(Cu), (c) Fe4-Fe2(Cu) and (d) Fe5-Fe2(Cu) in the clean GB and Cu-segregated GB models.

Figure 4 Charge density distribution of (1 $\bar{1}$ 0), (a) strain of 0% in the clean GB model, (b) strain of 10% in the clean GB model 10%, (c) strain of 20% in the clean GB model, (d) strain of 0% in the Cu-segregated GB model, (e) strain of 10% in the Cu-segregated GB model and (f) strain of 20% in the Cu-segregated GB model.

Figure 5 Charge density difference of (1 $\bar{1}$ 0) between the Cu-segregated GB model and the non-segregated GB model at the strain of 0%. In the non-segregated GB model, the Cu atom is replaced by a Fe atom with the same atomic configuration.

Figure 6 Charge density distribution of (2 $\bar{2}$ 0), (a) strain of 0% in the clean GB model, (b) strain of 10% in the clean GB model 10%, (c) strain of 20% in the clean GB model, (d) strain of 0% in

the Cu-segregated GB model, (e) strain of 10% in the Cu-segregated GB model and (f) strain of 20% in the Cu-segregated GB model.

Figure 7 Atomic partial density of states (PDOS) of the Fe1 atom at the strain of 0%, (a) the clean GB model and (b) the Cu-segregated GB model. The Fermi level is defined as the zero of energy.

Figure 8 Up- and down-spin partial density of states (PDOS) of *d*-bands for the Fe1 atom at the strain of 0%, where the solid curves show the PDOS in the clean GB model and the dashed curves show the PDOS in the Cu-segregated GB model. The upper and lower half parts indicate the up and down spin states, respectively. The Fermi level is defined as the zero of energy.

Table 1 Occupation numbers in $3d$, $4s$ and $4p$ electrons of the Fe1 atom in the clean GB model and the Cu-segregated GB model. Note that the $4s$ and $4p$ electrons play a vital role in the charge transfer.

	3d	4s	4p	all
Fe1 in the clean GB	6.638	0.733	0.886	8.257
Fe1 in the Cu-segregated GB	6.637	0.681	0.819	8.137

Table 2 Calculated magnetic moment (in units of μ_B) of each atom in the clean GB and Cu-segregated GB models.

Atom	clean GB model	Cu-segregated GB model
Fe1	1.940	2.060
Fe2(Cu)	2.780	-0.120
Fe3	1.940	2.100
Fe4	2.520	2.520
Fe5	2.380	2.500

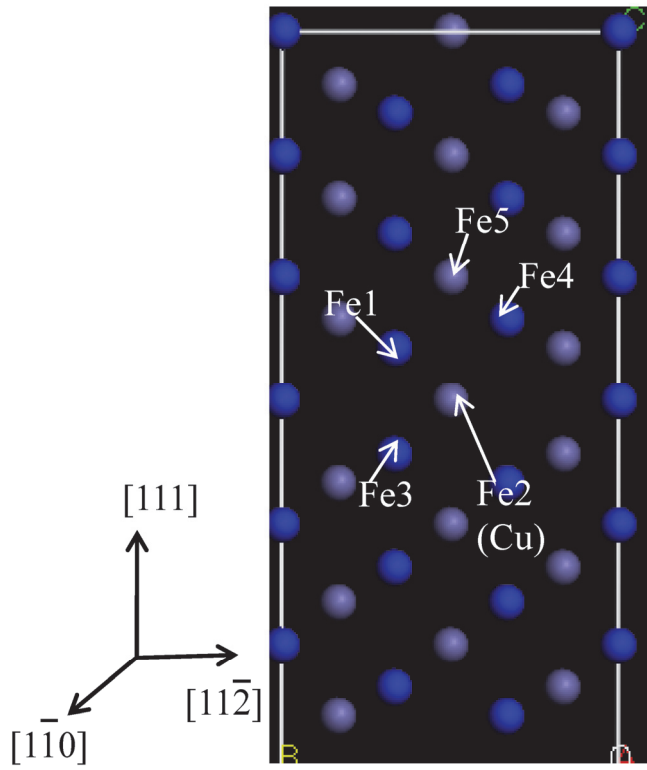


Figure 1 Unit cell model of Fe with a Σ_3 (111)/[11̄0] tilt grain boundary. In the present work, two cells are used: one is a cell without Cu segregation at the grain boundary (clean GB model) and the other is a cell with Cu segregation at the grain boundary (Cu-segregated GB model) in which an Fe atom (Fe2) at the grain boundary is substituted with a Cu atom. The initial cell size is $4.05 \times 7.02 \times 14.89$ Å. The blue and dark blue circles indicate the Fe atoms on the (11̄0) and the (22̄0) planes, respectively.

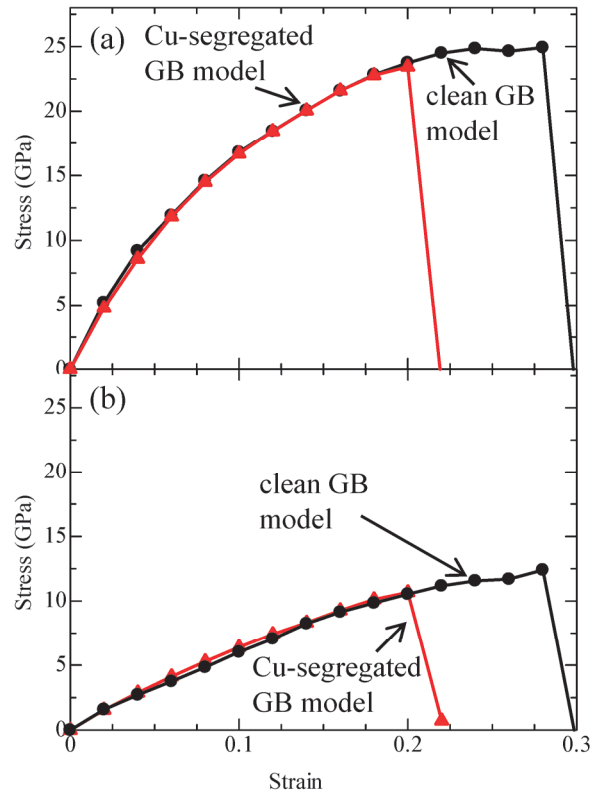


Figure 2 Stress-strain curves for the clean GB and Cu-segregated GB models, (a) [111] stress-strain curves and (b) $[11\bar{2}]$ stress-strain curves, where the [111] stress is the tensile stress in the [111] direction which is parallel to the tensile direction, the $[11\bar{2}]$ stress is the stress in the $[11\bar{2}]$ direction which is parallel to the GB and the strain is the strain in the [111] direction. Note that the tensile strength and the strain to failure in the Cu-segregated GB model are 8% and 27% lower than those in the clean GB model, respectively.

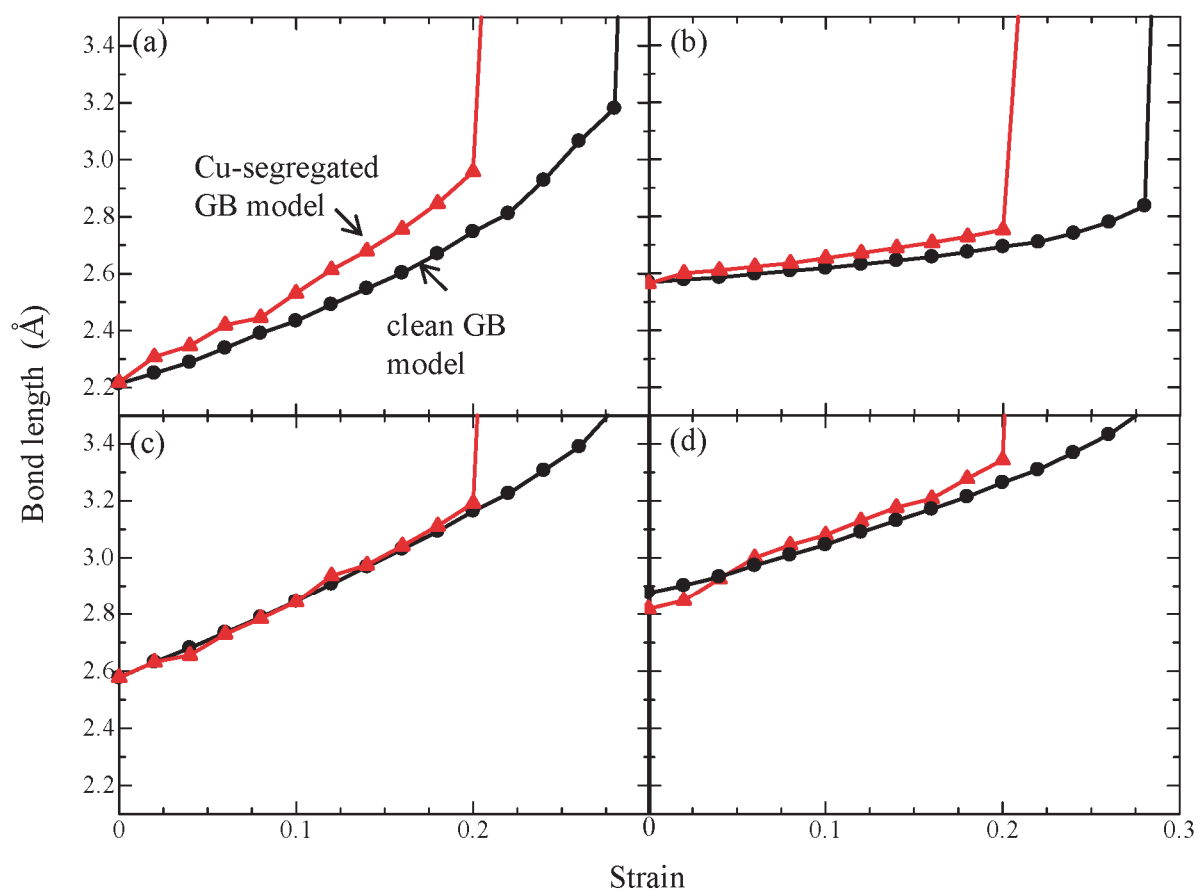


Figure 3 Variations in bond length as a function of strain, (a) Fe1-Fe3, (b) Fe1-Fe2(Cu), (c) Fe4-Fe2(Cu) and (d) Fe5-Fe2(Cu) in the clean GB and Cu-segregated GB models.

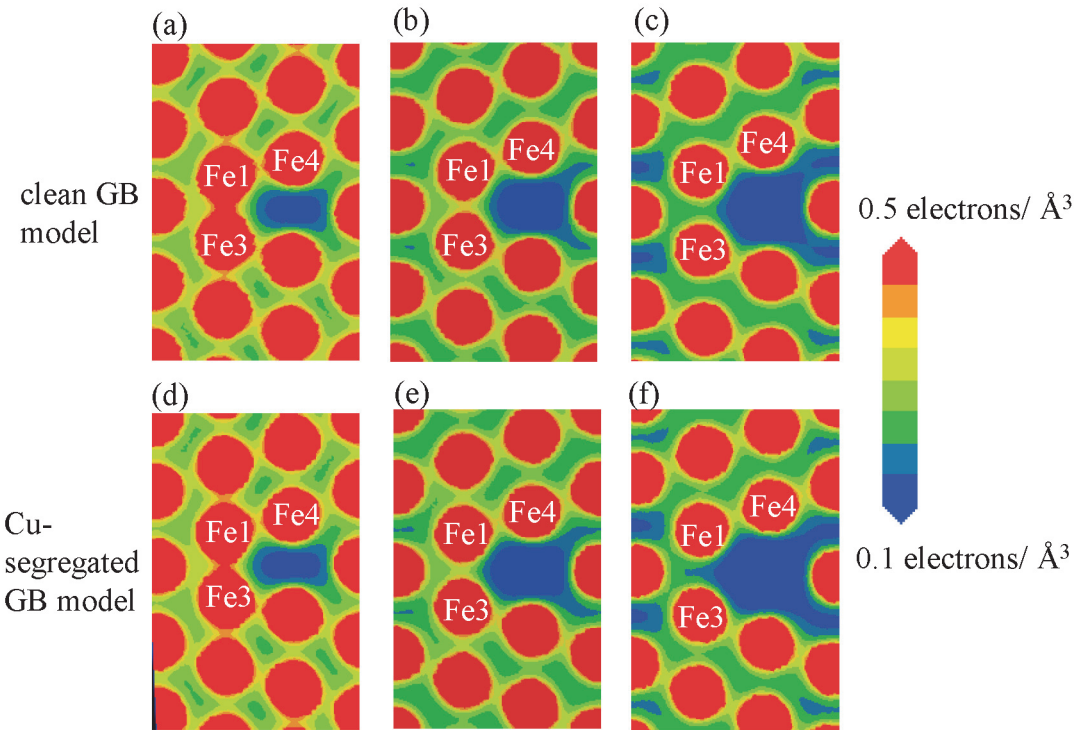


Figure 4 Charge density distribution of $(1\bar{1}0)$, (a) strain of 0% in the clean GB model, (b) strain of 10% in the clean GB model 10%, (c) strain of 20% in the clean GB model, (d) strain of 0% in the Cu-segregated GB model, (e) strain of 10% in the Cu-segregated GB model and (f) strain of 20% in the Cu-segregated GB model.

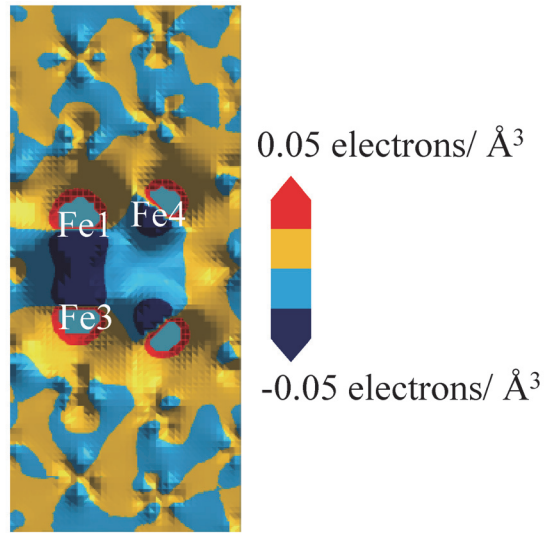


Figure 5 Charge density difference of $(1\bar{1}0)$ between the Cu-segregated GB model and the non-segregated GB model at the strain of 0%. In the non-segregated GB model, the Cu atom is replaced by a Fe atom with the same atomic configuration.

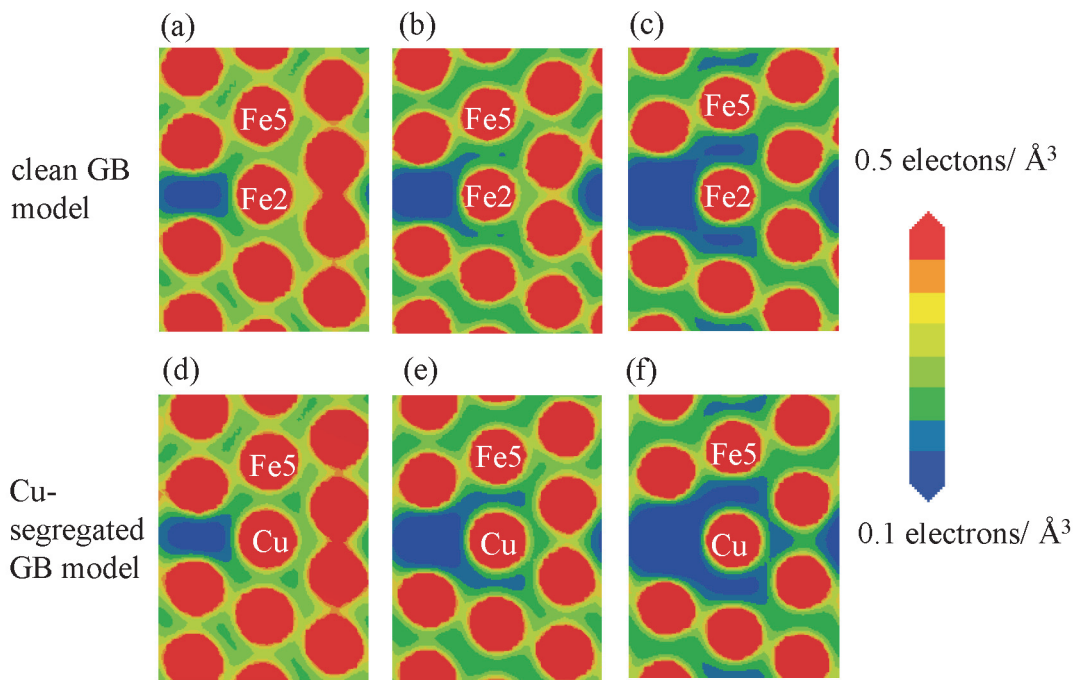


Figure 6 Charge density distribution of $(2\bar{2}0)$, (a) strain of 0% in the clean GB model, (b) strain of 10% in the clean GB model 10%, (c) strain of 20% in the clean GB model, (d) strain of 0% in the Cu-segregated GB model, (e) strain of 10% in the Cu-segregated GB model and (f) strain of 20% in the Cu-segregated GB model.

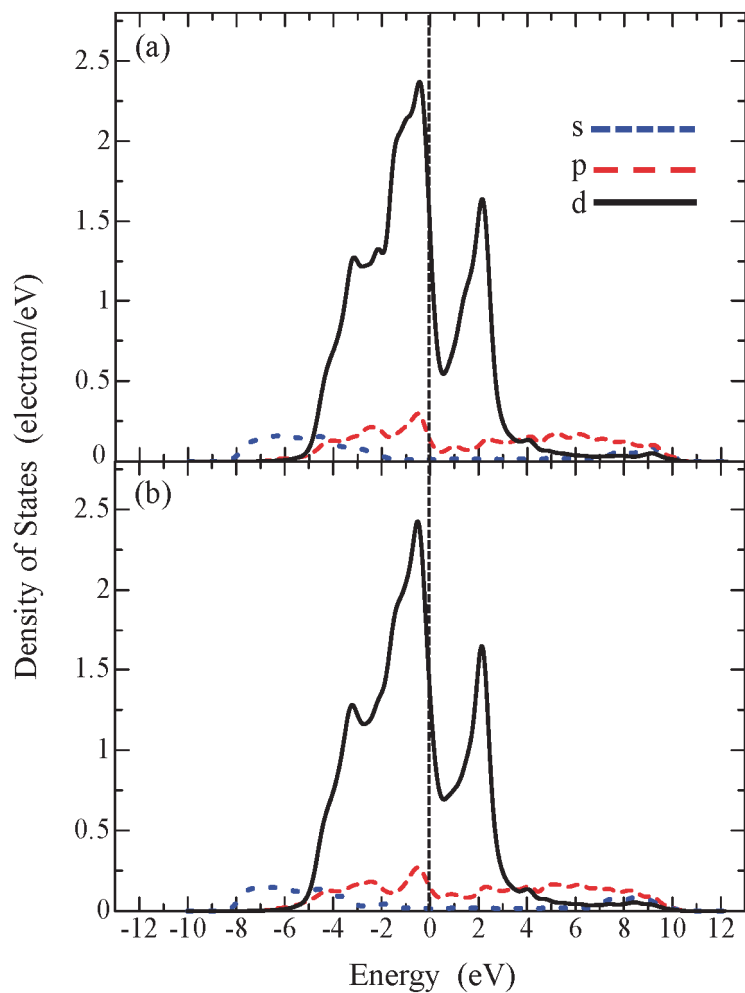


Figure 7 Atomic partial density of states (PDOS) of the Fe1 atom at the strain of 0%, (a) the clean GB model and (b) the Cu-segregated GB model. The Fermi level is defined as the zero of energy.

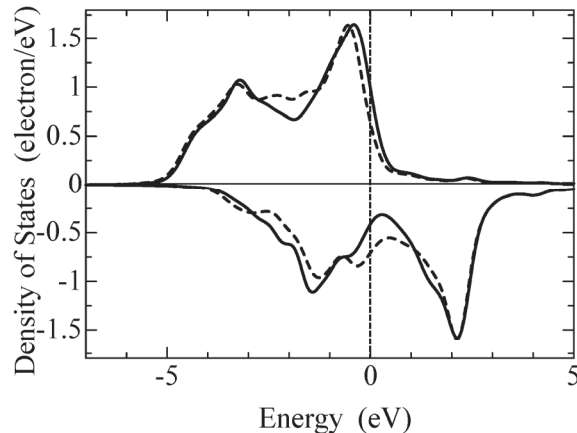


Figure 8 Up- and down-spin partial density of states (PDOS) of d -bands for the Fe1 atom at the strain of 0%, where the solid curves show the PDOS in the clean GB model and the dashed curves show the PDOS in the Cu-segregated GB model. The upper and lower half parts indicate the up and down spin states, respectively. The Fermi level is defined as the zero of energy.